



The EFI of onboard THEMIS Satelite mission

2020.6.19
Xian-Ming Zheng



1. Resume

2. Introduction

3. formulation and design

4. First results

5. Summary



Resume

Education experience

2012.9~2016.6,(Ningbo university),Electronic science and technology
Bachelor degree



2016.9~2019.7,(University of science and technology of China-USTC),
optical-lidar master degree



2019.6~2020.1,(Institute of military sciences) ,Microwave photonic radar
design a photonic radar - had completed

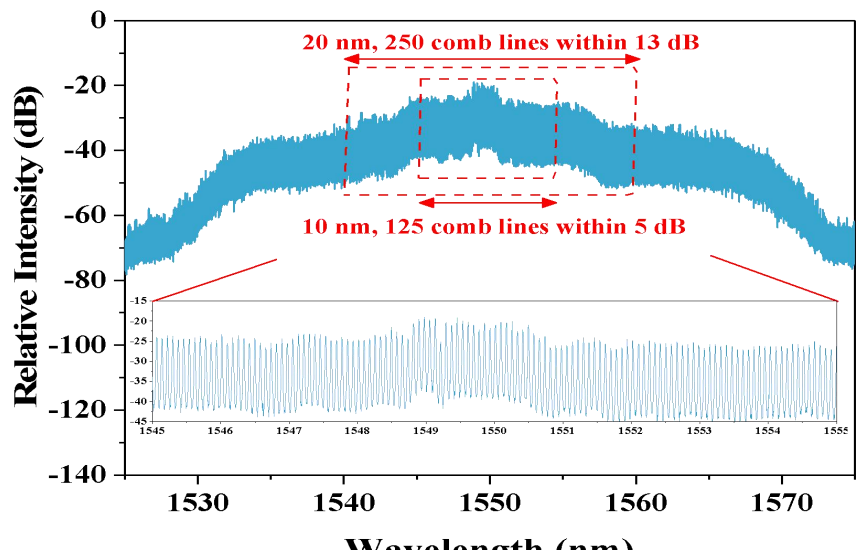
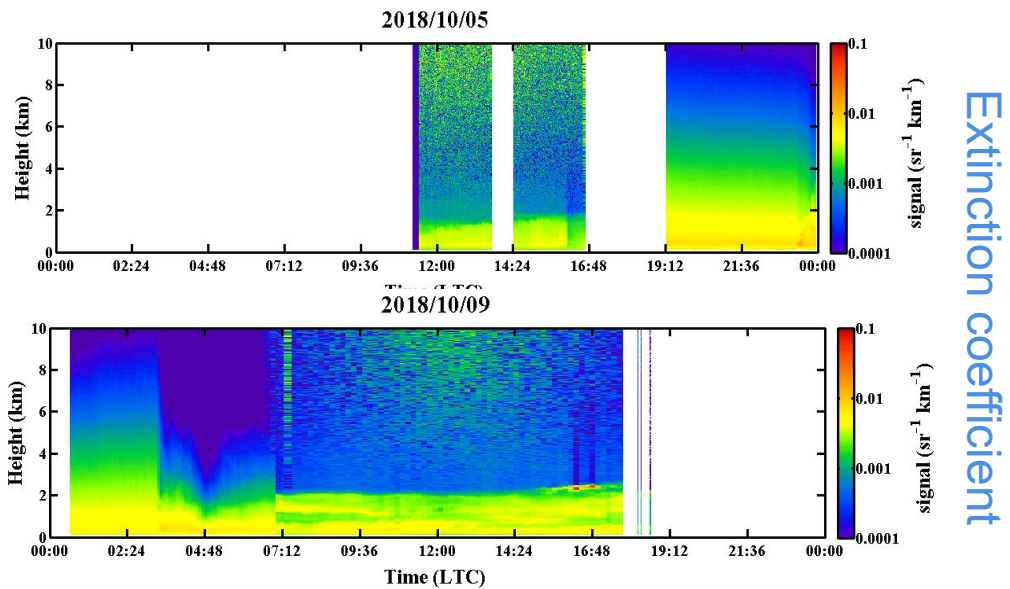
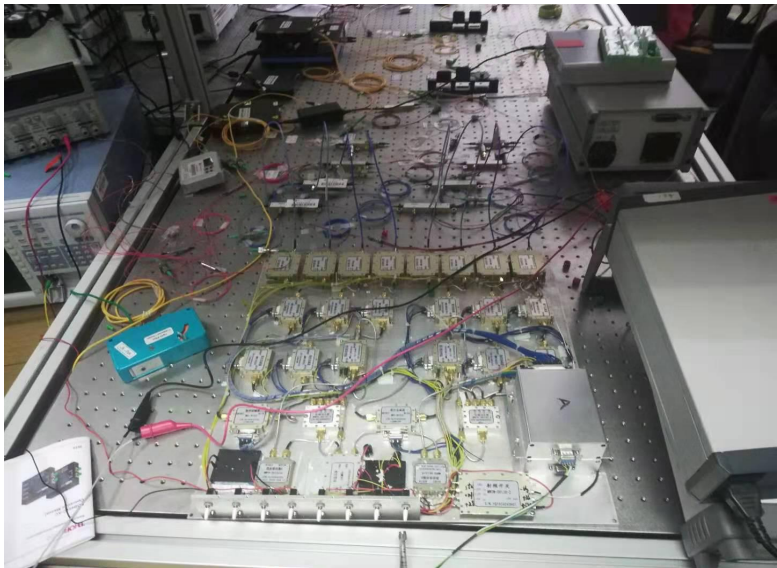
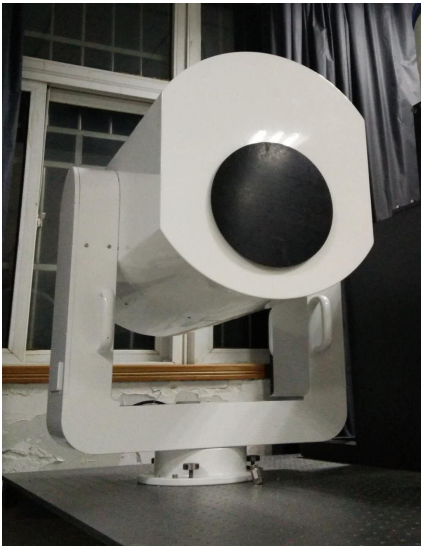


Research direction

Automatic control, software development, data processing



Resume





Section2 intruduction

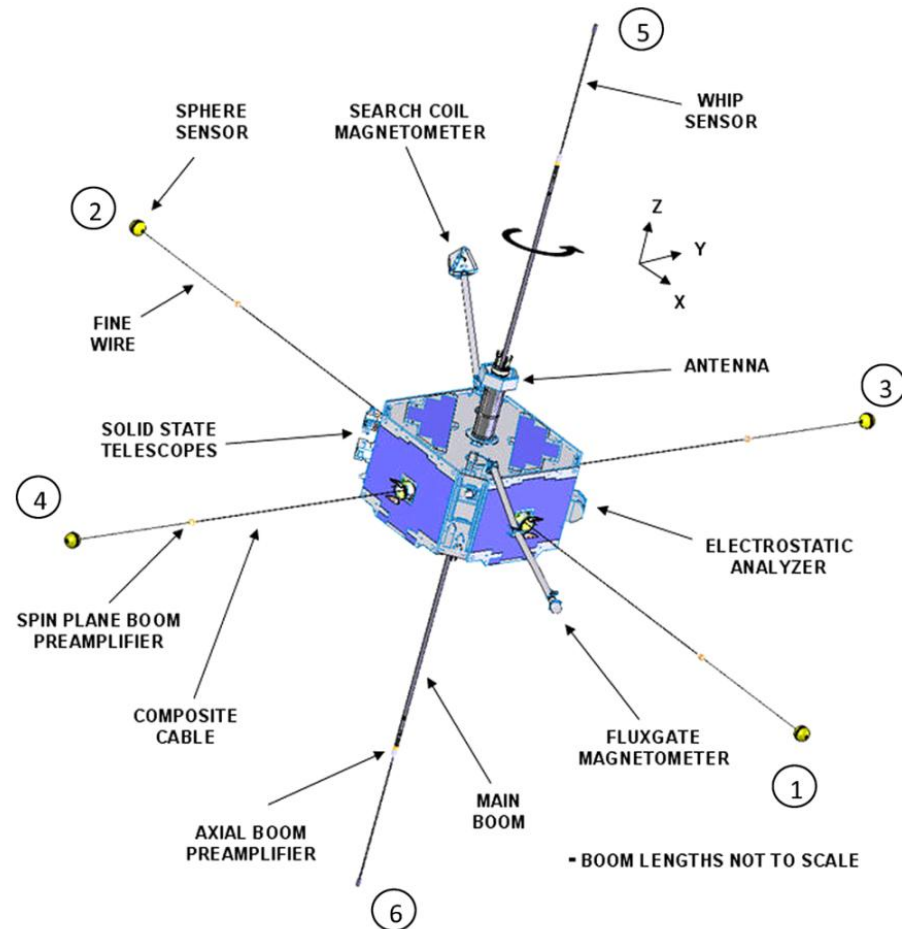


Fig. 1 Schematic diagram of THEMIS spacecraft, including body- and boom mounted sensors

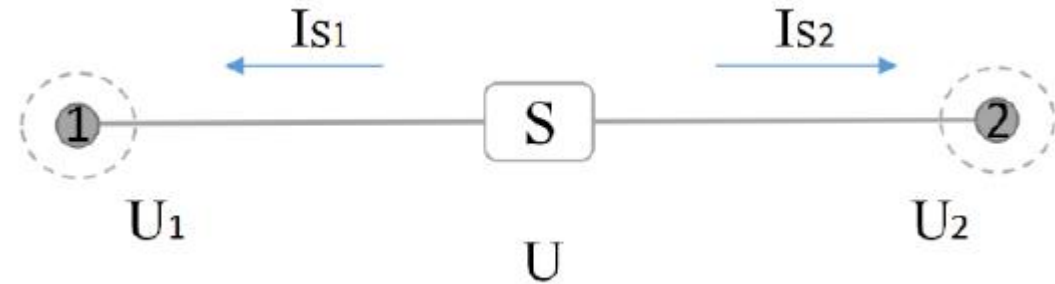
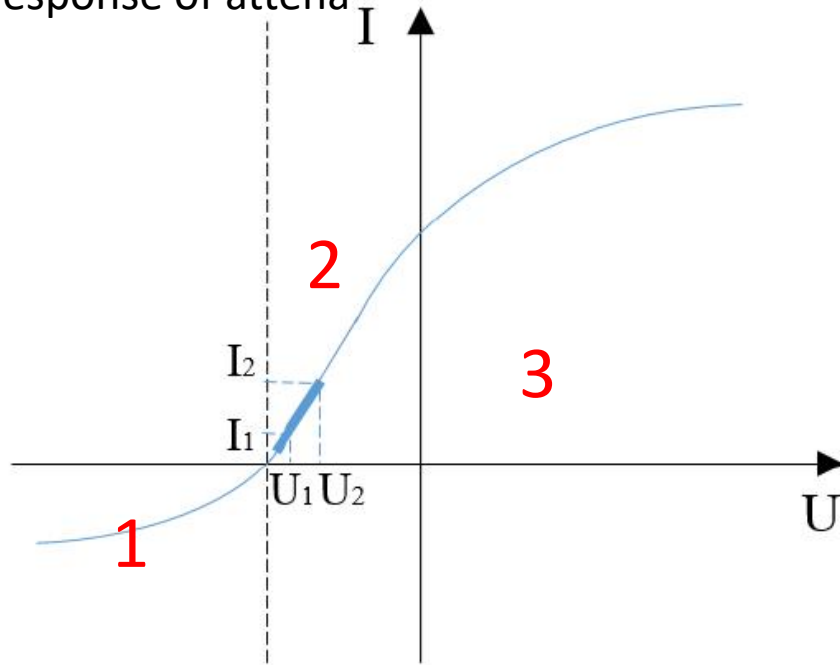
1. The EFI have six sensors , the individual sensor are identified by number (1-6).
2. any one individual sensor potentials can be measured (V_n , $n=1, \dots, 6$).
3. Both individual and differential can be calculated ($E_{mn} = V_m - V_n$), $m, n=[12 \ 34 \ 56]$).



Section2 formulation and design

Principle of measurement:

V-A response of antenna



$$E_1 = (U_1 - U_2)/L$$

$$E_2 = \frac{U_1 - U_2}{L} - V \times B$$

U_1, U_2 respectively probe the measured potential.

L are two probe center spacing.

V is flat Machine speed.

B as the earth's magnetic field.

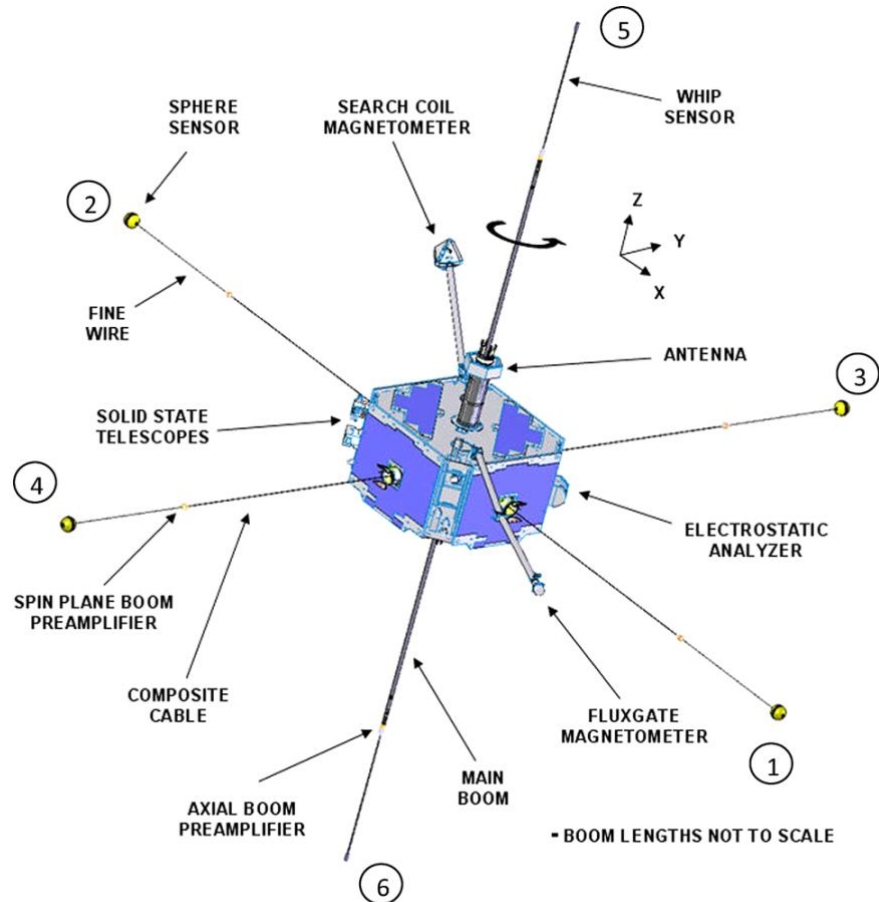
E electric field for the space.

$$E_v = V \times B \longrightarrow \text{Induced electric field}$$



Section3 formulation and design

Mechanical design:



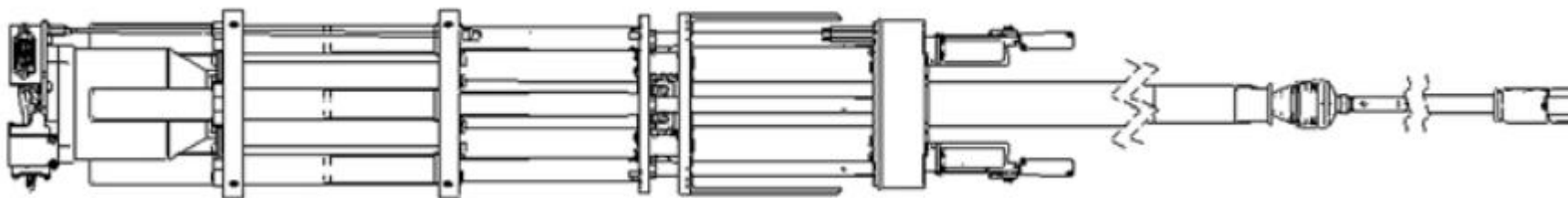
1. 1~4 are rotary plane electric field meters, which are connected by the above flexible cable.
2. 5 and 6 are rotary axial electric field meters, which are connected by rigid folding extension rods.

Fig. 1 Schematic diagram of THEMIS spacecraft, including body- and boom mounted sensors



Section3 formulation and design

Mechanical design: Bracket with folding extension rod



Parameter:

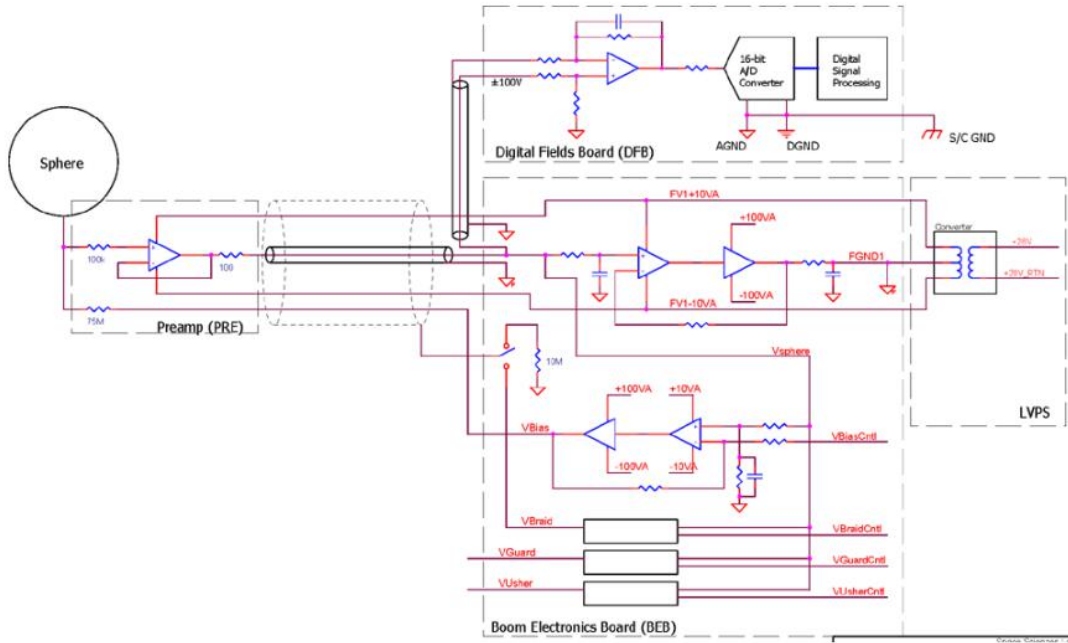
1. with the frequency range of DC~8kHz
2. which can be reached by a single broadband channel
3. The accuracy is better than 1mV/m, Individual bandwidth up to 400KHz

Axis	Deployed length	Notes
X (V1, V2, E12)	49.6-m tip-to-tip	None
Y (V3, V4, E34)	40.4-m tip-to-tip	None
Z (V5, V6, E56)	6.93-m tip-to-tip	0.76-m whip length; ≈6.2-m whip center-to-center



Section3 formulation and design

Electric design : there are contain three sections



1. Digital Fields Board (DFB)
2. Boom Electronics Board (BEB)
3. Low-Voltage Power Supply (LVPS)
4. located in the central Instrument Data Processing Unit (IDPU)

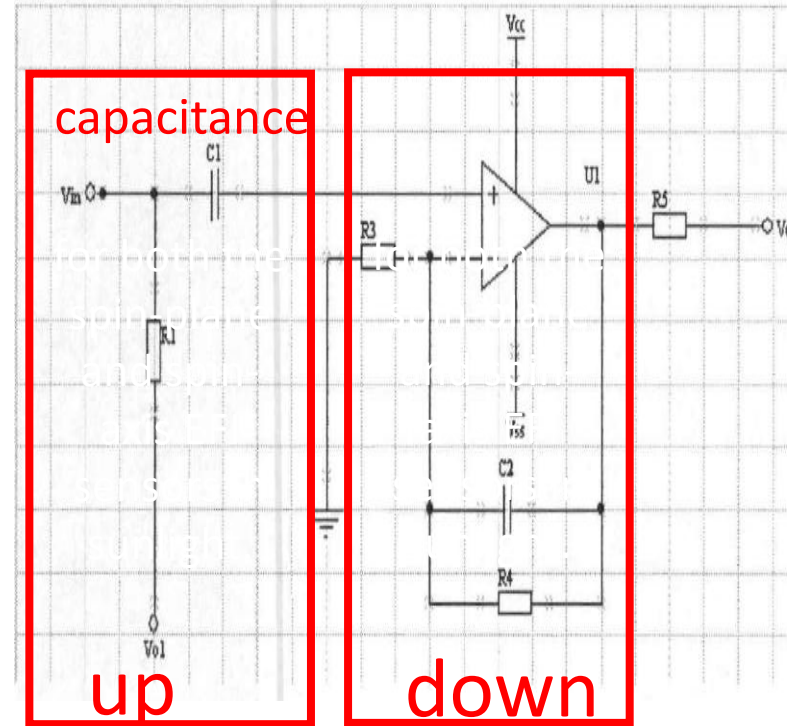
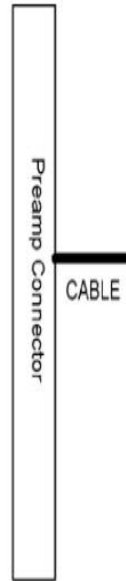
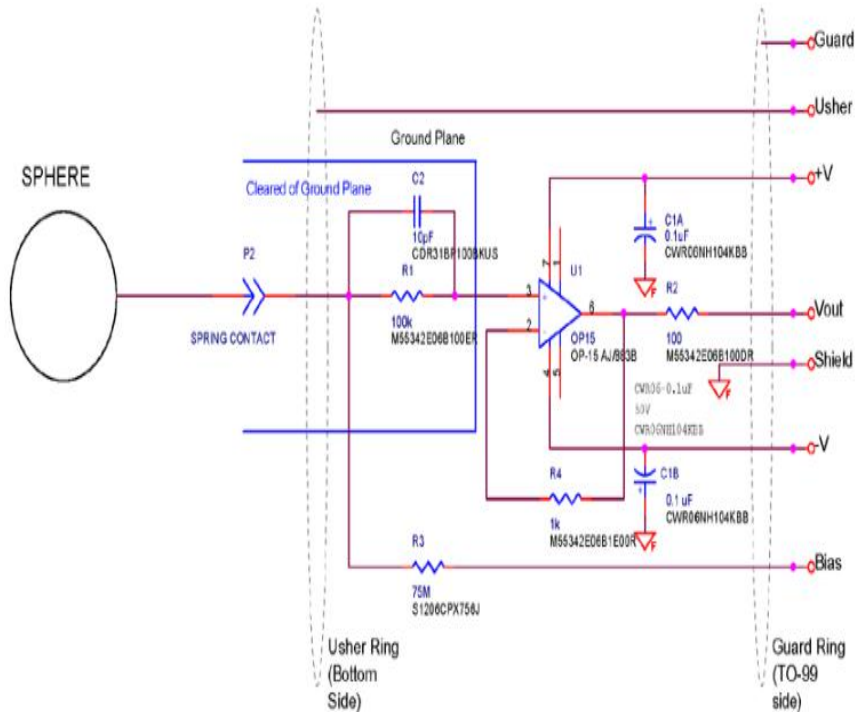
All of the construct of IDPU circuit

Each sensor electrode is connected to the input of high-input-impedance ($\sim 10^{12}$ ohm), low-noise unity-gain preamplifier circuit



Section3 formulation and design

Electric design: AC preamp circuit, , now day's only a FPGA board can achieve it



$$VCC = \pm 10v$$

$$f=100\text{HZ}$$

$$R_1=100K\Omega$$

$$C_1 = 10pF$$

$$R_2=100\Omega$$

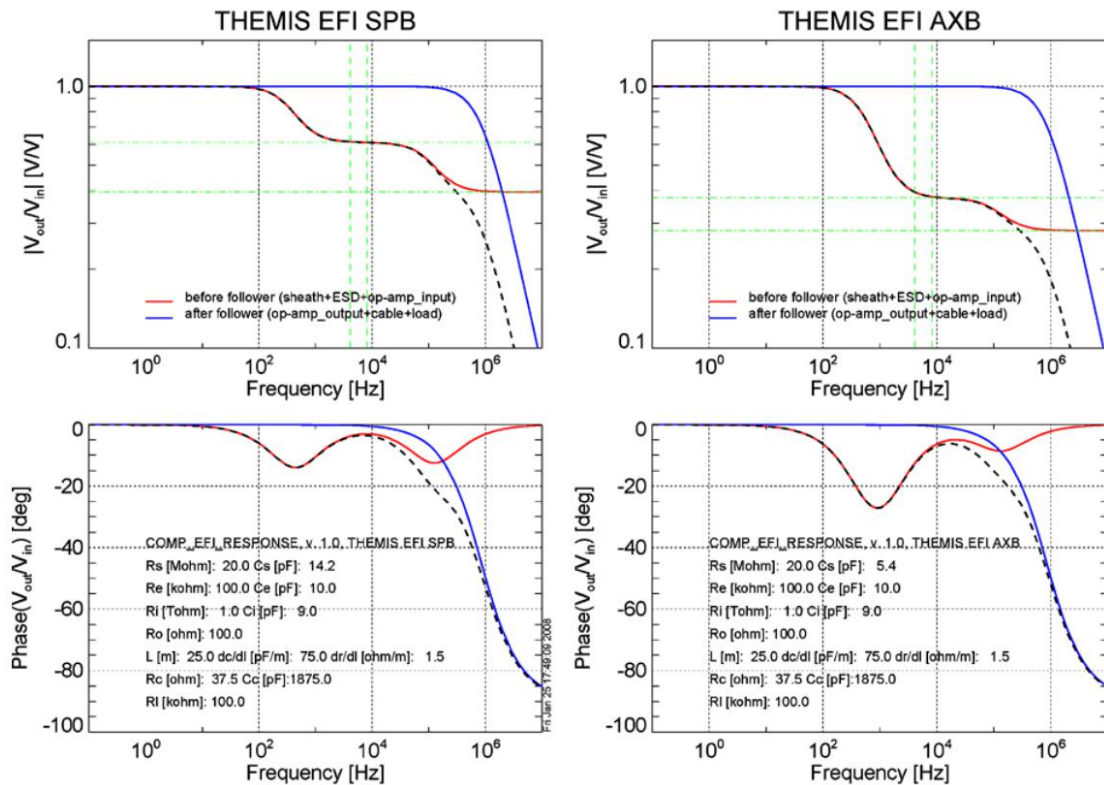
$$C_2 = 2nF$$

For the CD part, it contains a strong induced electric field, no preamplification is done, and the signal is directly led to the electronics box.



Section2 formulation and design

Electric design: both the spin-plane and spin-axis EFI sensors in sunlight



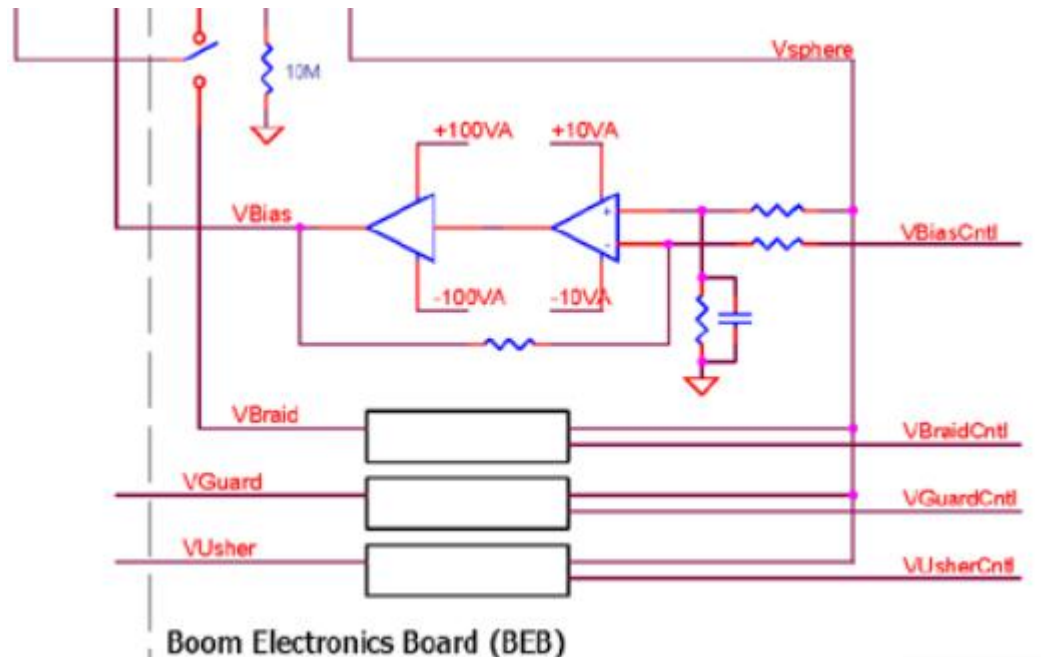
1. This shows the predicted frequency response (voltage gain and phase)
2. The total response is denoted by the black dashed line.
3. the contributions to the response for circuit elements upstream and downstream (red and blue lines)

Fig. 7 Predicted frequency response of THEMIS-EFI spin-plane and spin-axis antennas



Section3 formulation and design

Electric design : boom electronics board (BED)



BEB is controlling :

1. floating grounds($\pm 60V$ range).
2. Current and voltage($\pm 40V$ potential) bias signals sensors.(16 bit ADC)
3. DBRAID reference selection(400-Hz low-pass-filtered)

- 11–12 bits of the total DAC resolution is required to implement the 0.1% precision.
- the remaining 4–5 bits acting as margin in case of DAC degradation over time.



Section3 formulation and design

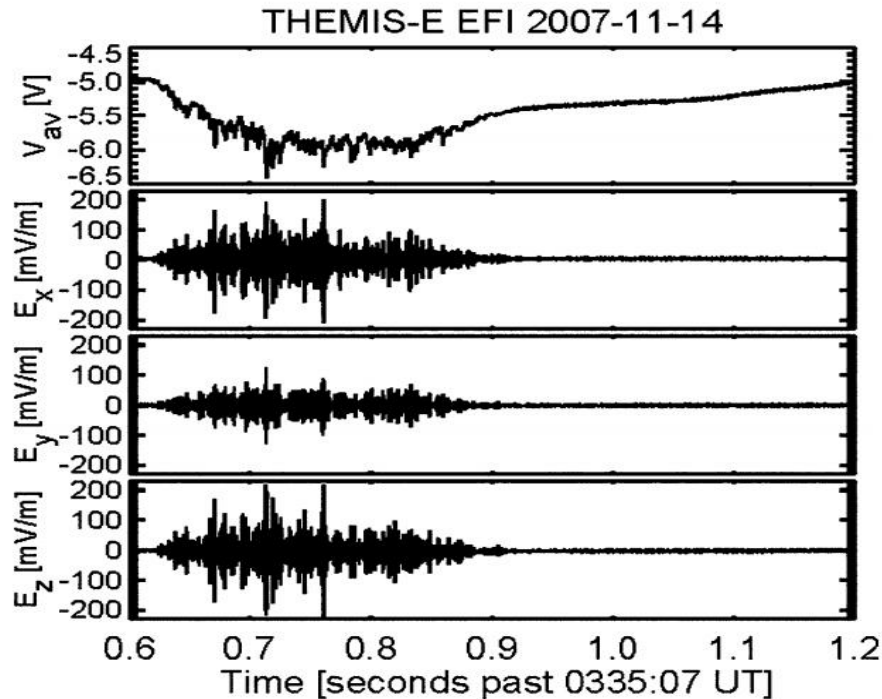
Electric design : Data characteristic conclusion

1. DC-coupled channels have a DC CMRR of better than 80 dB (better than 0.1 mV/V common mode input).
2. AC coupled channels have a AC CMRR of better than 40 dB (10 mV/V common mode input) .
3. For the spin-fit E_{xy} , the DC-coupled E12 or E34 channel is fit to a model of the form:
 $A+B \cdot \sin(\psi)+C \cdot \cos(\psi)$, where ψ is spin phase relative to the Sun pulse.
4. data quantities 、 dynamic ranges、 precision、 and other properties are determined by the analog and digital signal processing performed by the DFB.

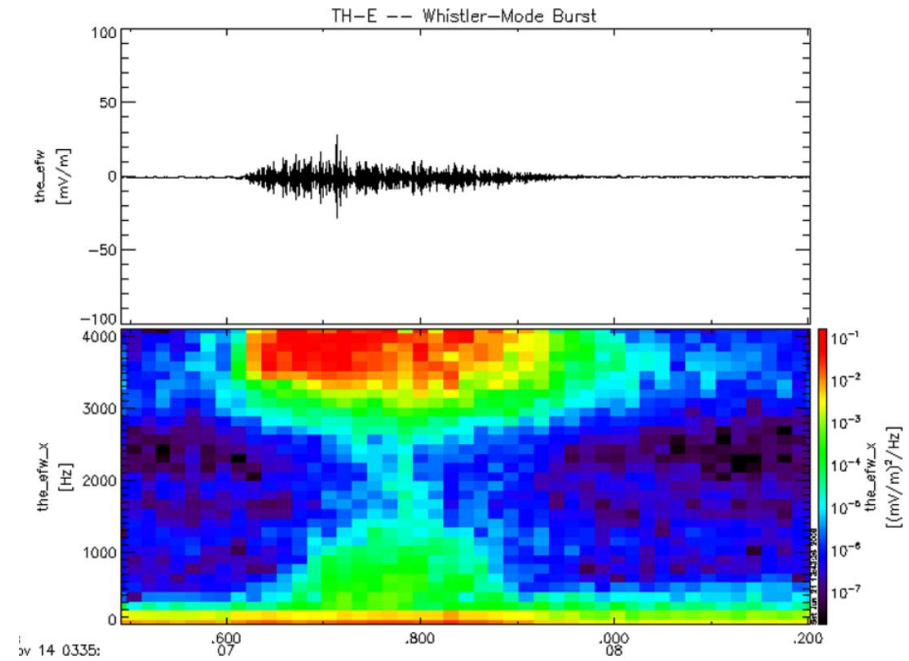


section3 First results

Large-Amplitude Whistler Wave Observations in the Radiation Belt



1. Spacecraft floating potential(-0.65V- -0.5V).
2. E-field showing large amplitude (200–400 mV/m, pk-to-pk).

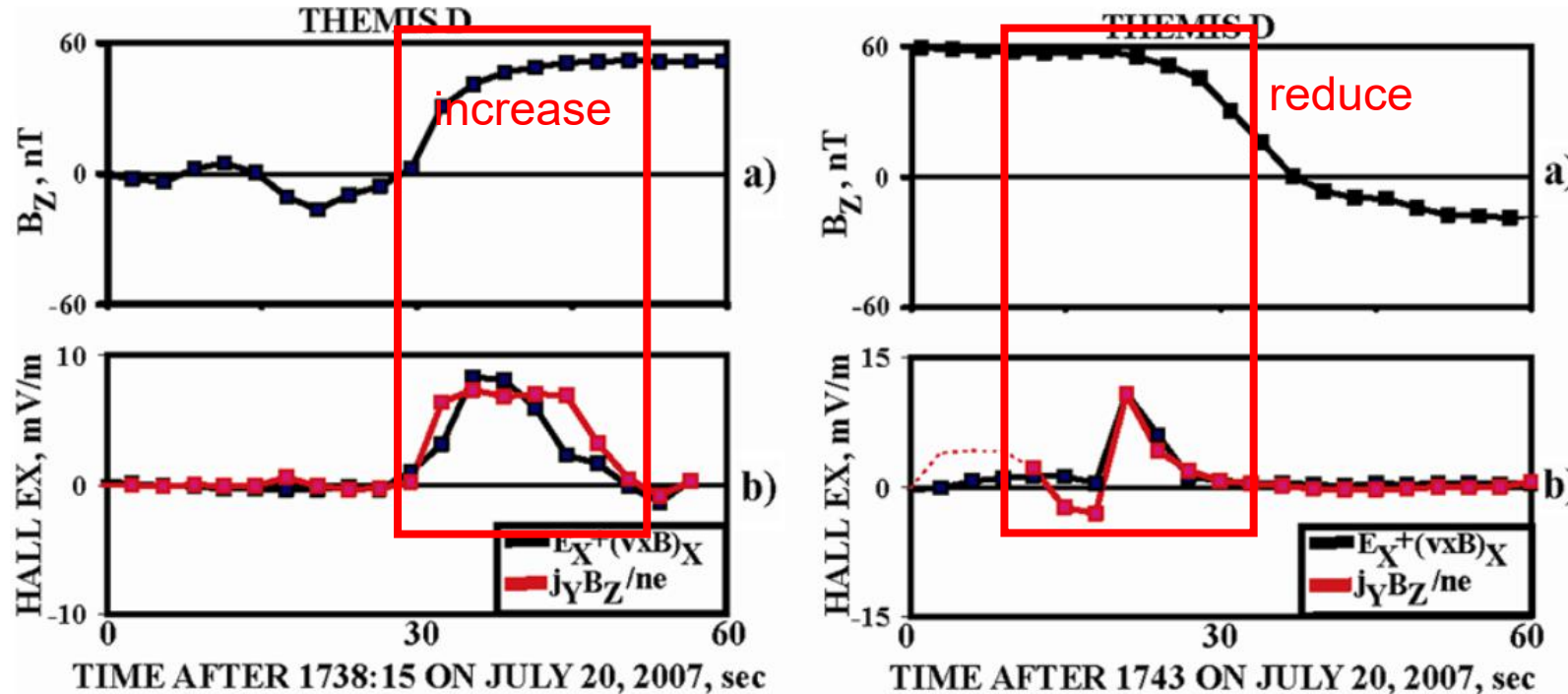


1.

it can be shown that the **upper- and lower-band** hiss in the inner magnetosphere consists primarily of spatially or temporally-localized bursts of these large-amplitude whistler-mode fluctuations.



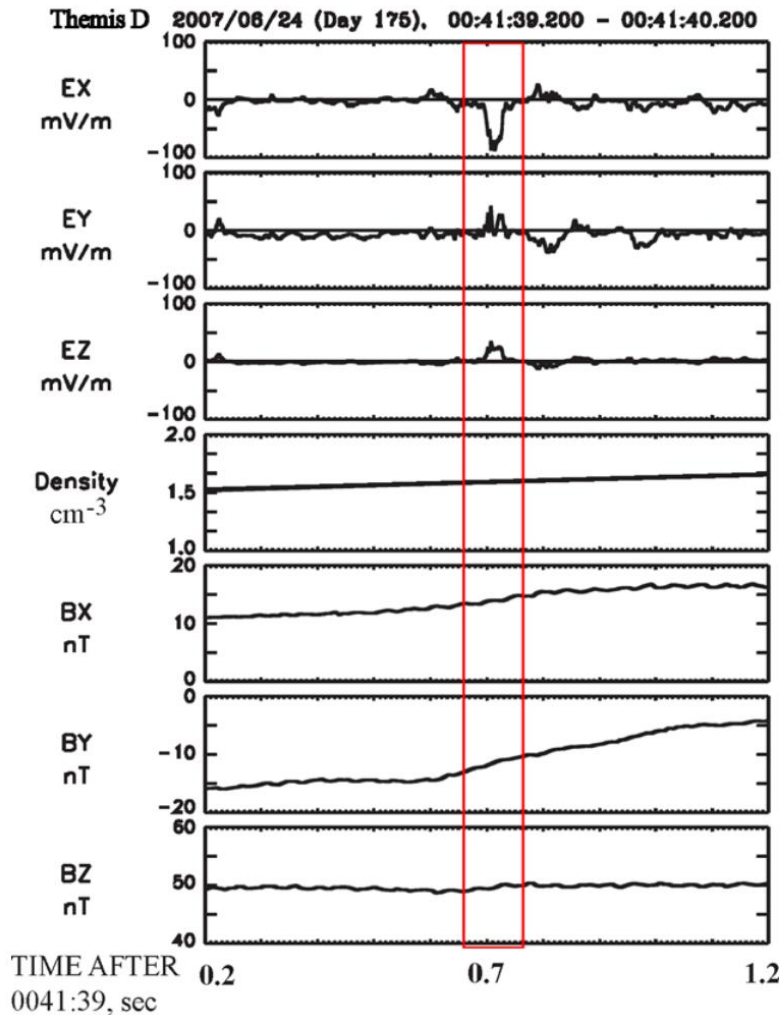
section3 First results



1. Hall Electric Field Observations at the Magnetopause.
2. the Hall field occurs on the magnetospheric (low-density, high- B) side of the magnetopause.
3. This asymmetric distribution of the Hall E -field has been shown to be consistent with the predictions of the generalized Ohm's law.



section3 First results



1. at 0.7 s into the interval .
2. the size of this region is less than 1 km .
3. continuous about 30 ms in this region



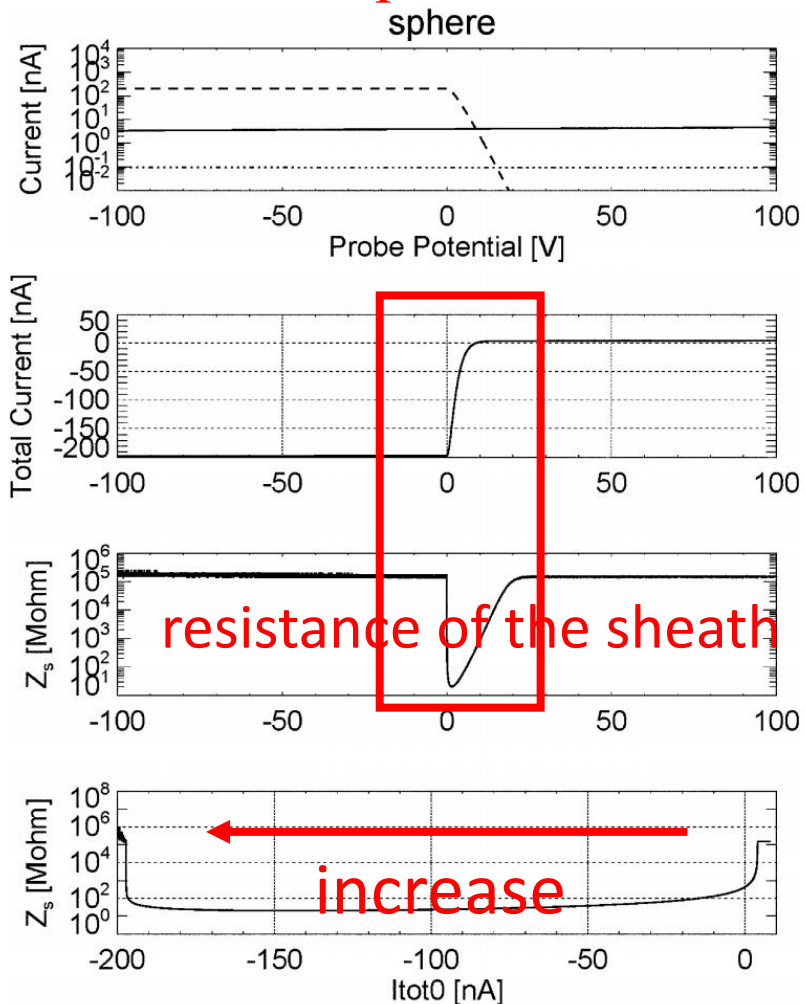
the spacecraft was passing from the magnetosphere into the magnetosheath


Electron Diffusion Region-Scale \mathcal{E} -Field Structures at the Dayside Magnetopause



section4 Performance and Operation

On-Orbit Bias Optimization:

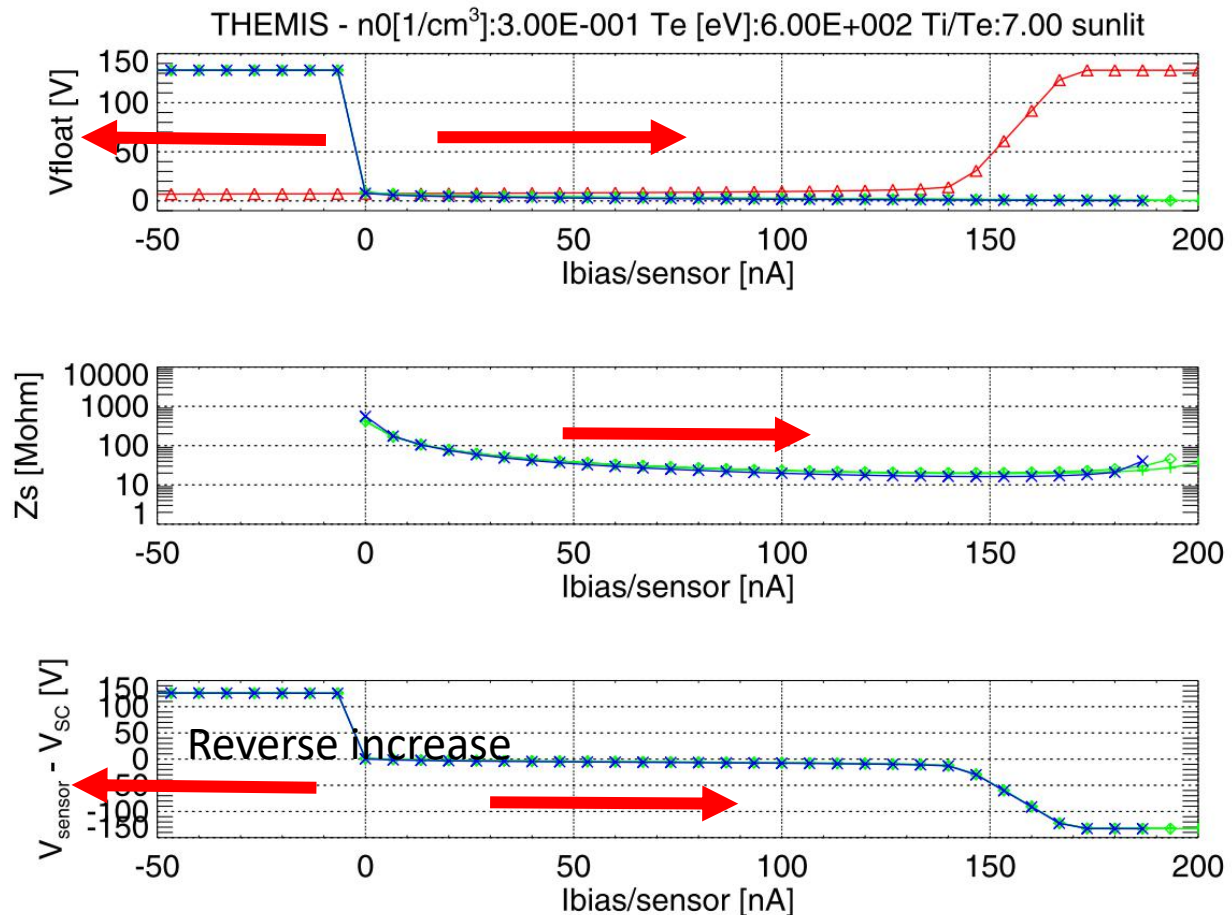


1. The topmost panel shows the contributions from the photoelectrons.
2. The top two panels show the current as a function of potential difference between the sensor and the local plasma potential.
3. The third panel shows the small-signal resistance of the sheath, and potential to variations in current due to either changes in the ambient plasma conditions.
4. The fourth panel shows this sheath resistance as a function of bias current to the sensor.
  Suitable I bias
 this way can reduce the error voltage from 100mV-1mV



section4 Performance and Operation

On-Orbit Bias Optimization:

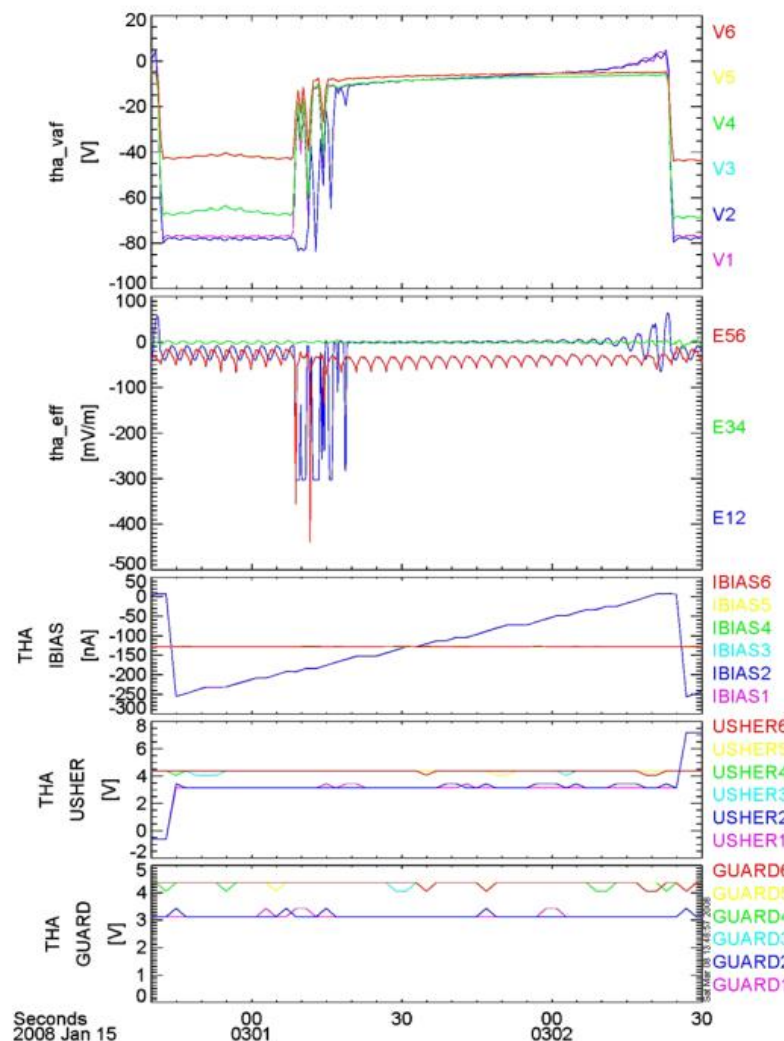
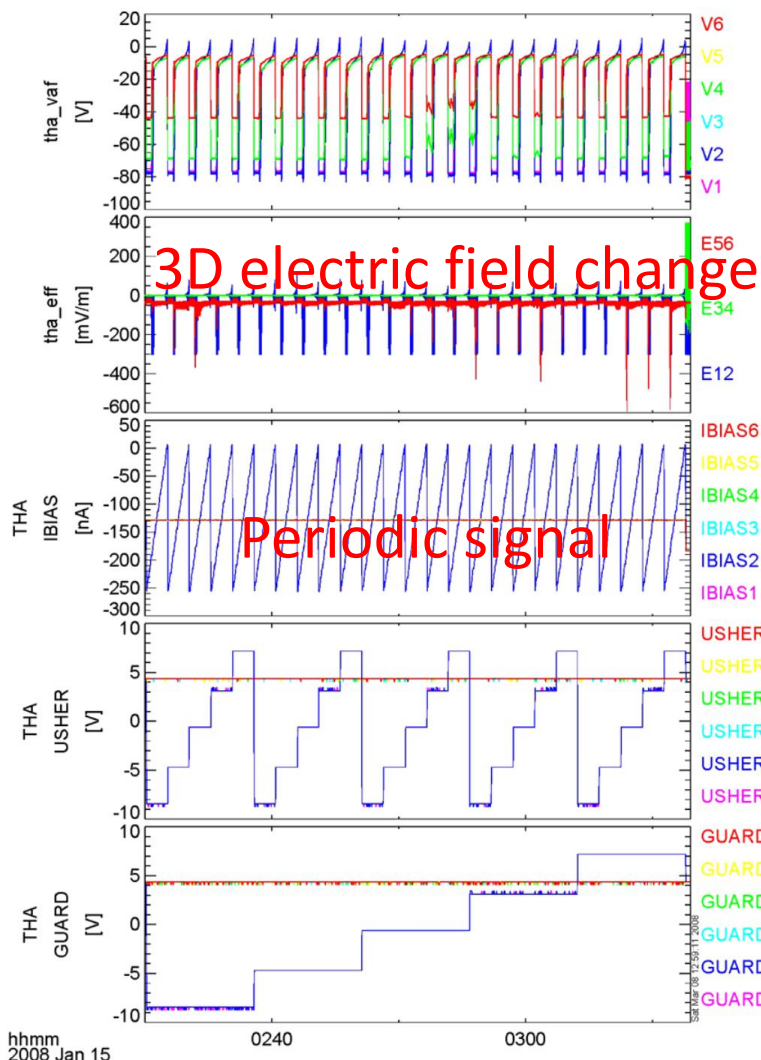


1. EFI sensor and spacecraft floating potentials (*top panel*).
2. sheath resistances (*middle panel*).
3. sensor relative to spacecraft potentials (*bottom panel*) as a function of bias current.



section4 Performance and Operation

Sensor Diagnostic Tests: (SDT)

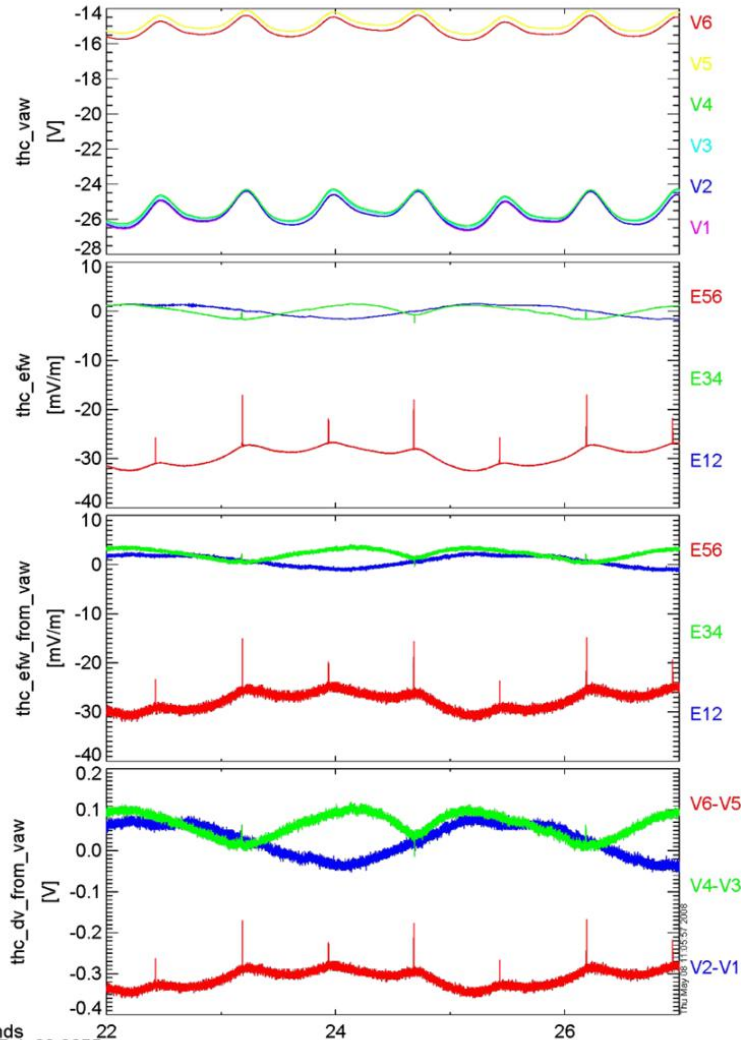


1. The left panel shows the entire SDT run on the X-axis sensors.
2. the right panel zooms in on one IBIAS sweep to show the variation in sensor potential and sensitivity to stray photoelectron currents with bias current .



section4 Performance and Operation

Spacecraft Potential Variations:



1. The top panel shows the six individual sensor potentials relative to spacecraft ground.
 2. the middle panel the three E on-board DC-coupled differential channels.
 3. the bottom panel the equivalent differential measurements computed on the ground from the individual sensor potentials.
- The highest rate (8192 samp/s wave burst data; vaw and efw) data products are used in this comparison to bring out the finest scale features of the potential variations.



section4 Performance and Operation

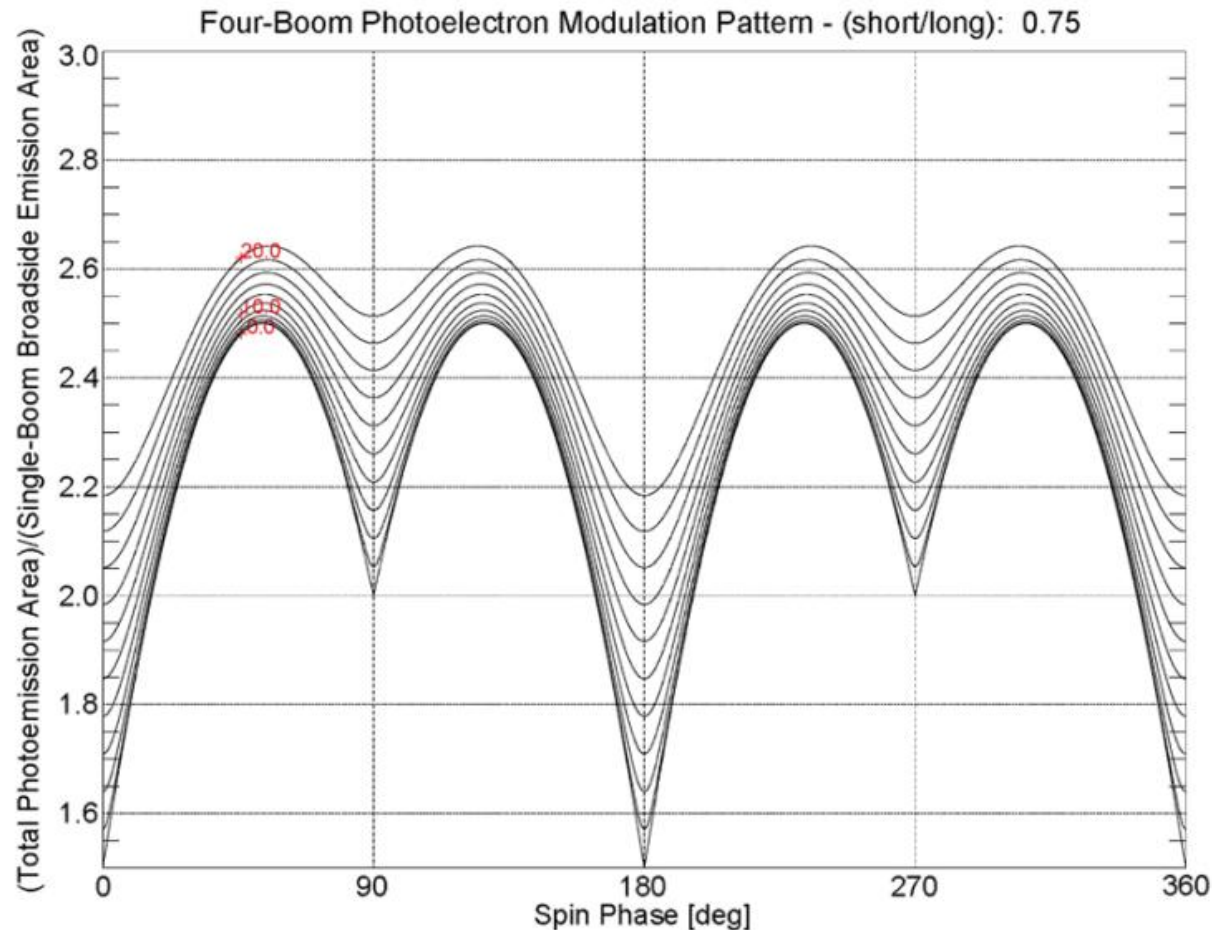


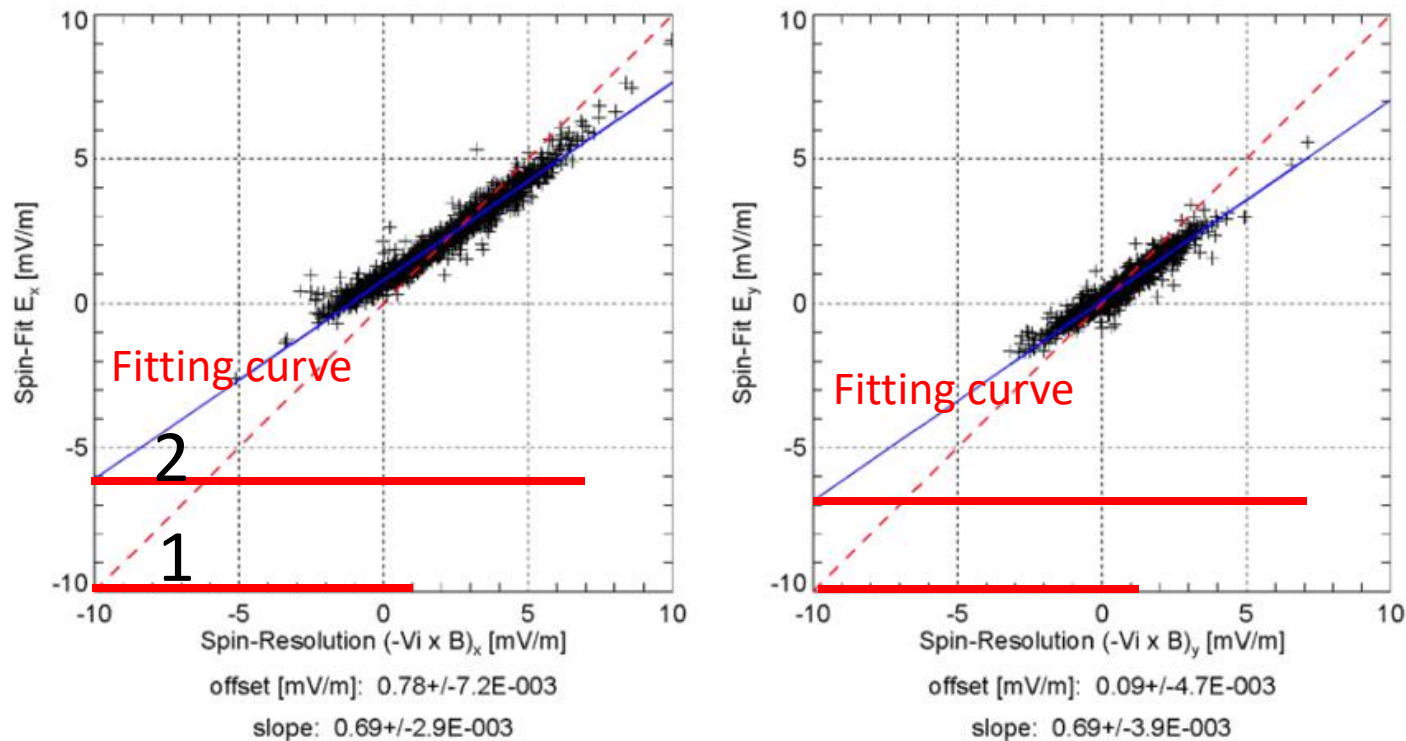
Figure shows the expected variation of this emission area as a function of spin phase and Sun angle (minimum angle of Sun with respect to spin plane), which matches quite well with the observed variation.

essentially, the axial sensors are ≈ 10 times closer to the center of potential, and see a smaller floating potential because of that difference.



section4 Performance and Operation

Cross-Calibration and Determination of Boom Shorting Factors



conditions : the external electric, magnetic, and plasma flow fields are uniform and quasi-static, and the fluids themselves are collisionless, then the fields and flows are related by the standard ideal MHD.

conclusion : $\mathbf{E} = -\mathbf{V}_i \times \mathbf{B}$.

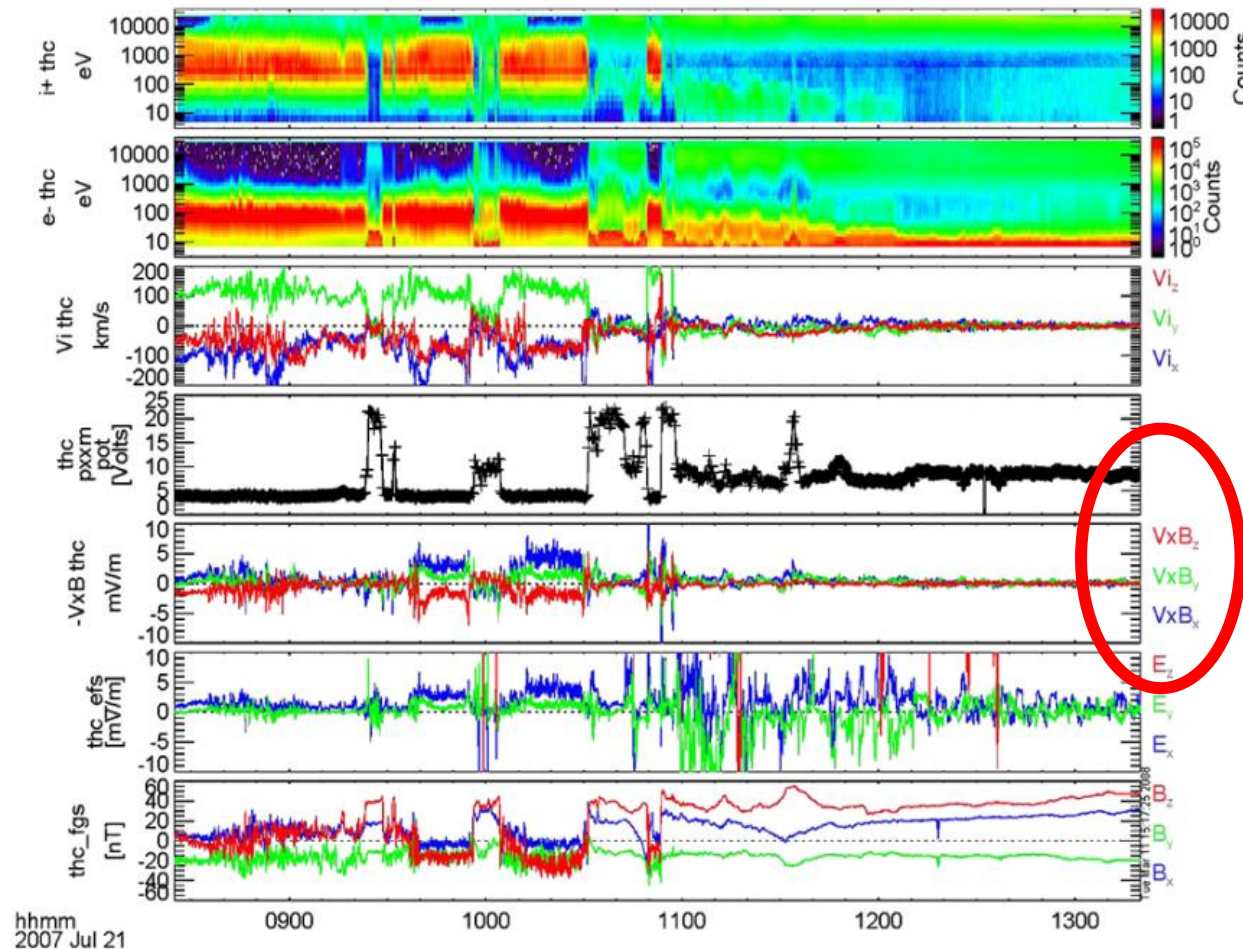
$$E_{EFI} = V_{iESA} \times B_{FGM}$$

Fig. 21 Correlation analysis between EFI, iESA, and FGM data in the magnetosheath



section4 Performance and Operation

Electrostatic Wake Effects

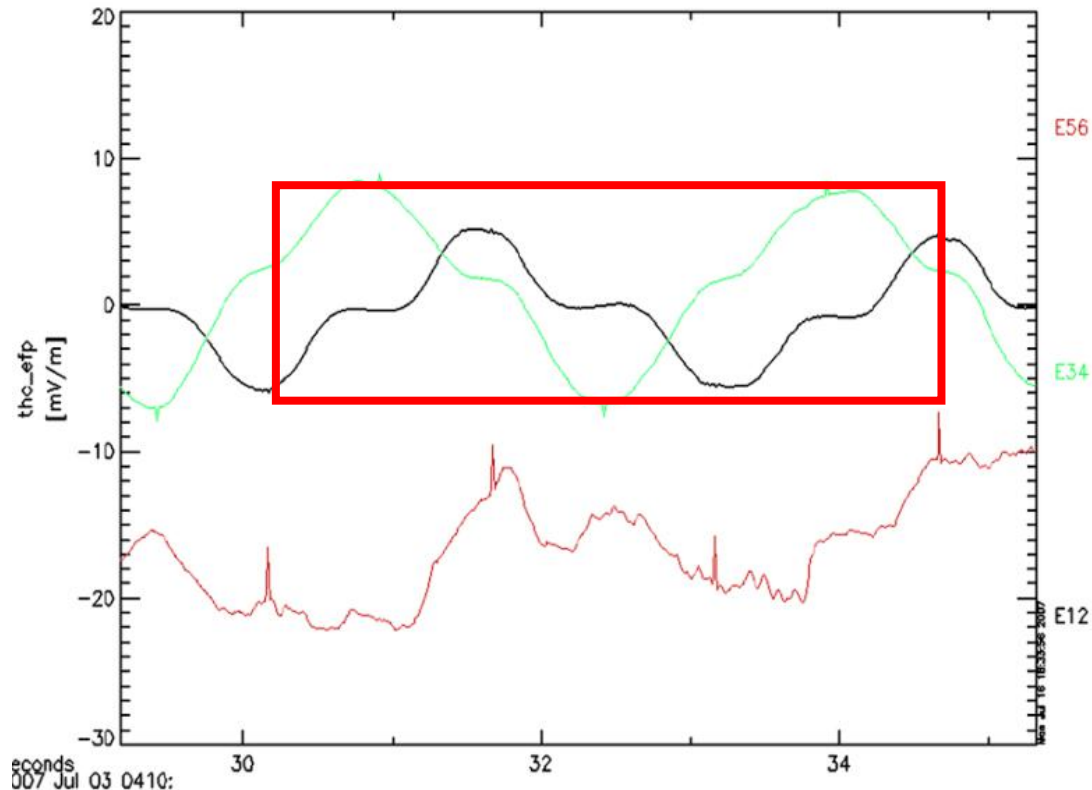


1. The **top two panels** show the ion and electron count rates (proportional to differential energy flux) as a function of energy.
2. The **third panel** shows the ion velocity in despun spacecraft coordinates.
3. The **fourth panel** shows the estimated spacecraft floating potential.
4. The fifth and sixth panels show the estimated E -field from spin-resolution - $V_{i_{ESA}} \times B_{FGM}$ **and** E_{EFI} .
5. the **seventh panel** shows the spin-fit **B**.



section4 Performance and Operation

Electrostatic Wake Effects



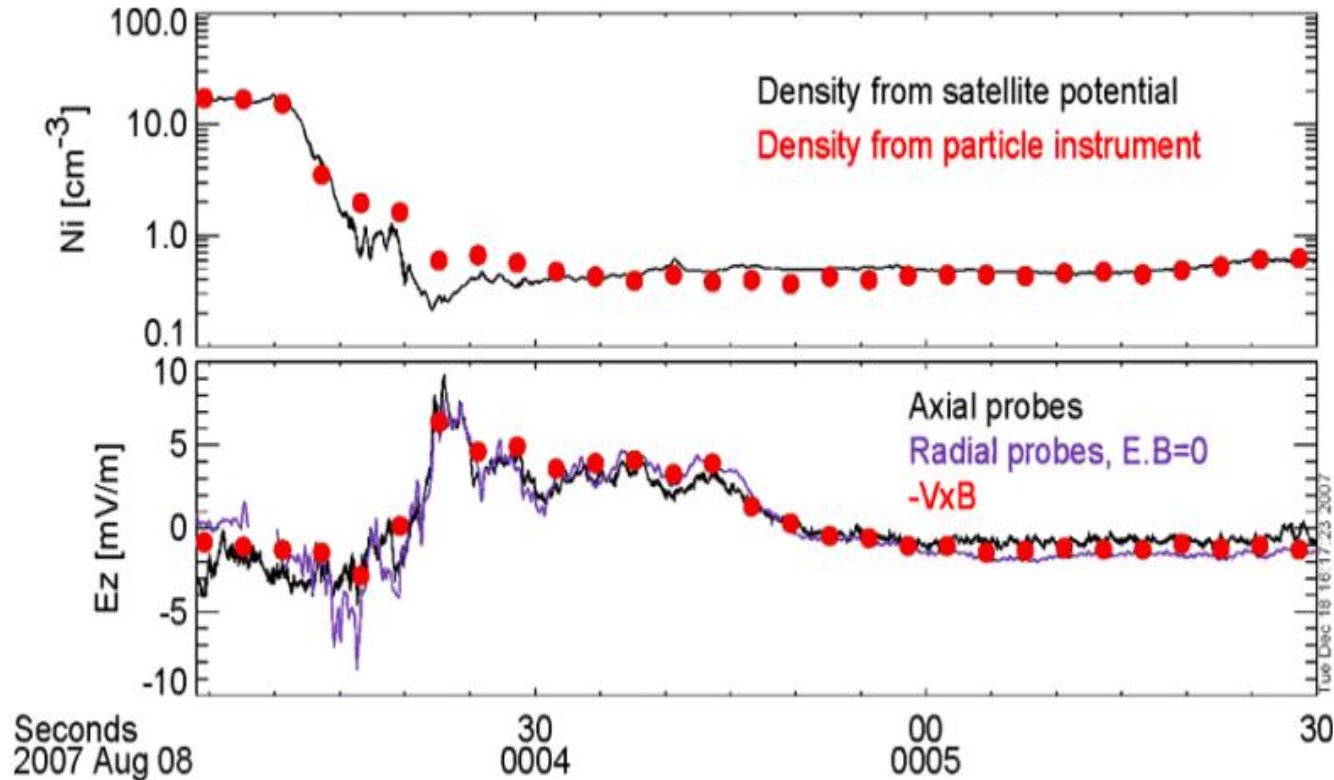
Spin plane (*black, green*) and axial (*red*) E -field measurements during cold plasma wake event .

Question:

1. Unlike the signal from a uniform external E -field (L , as $1/L2$ or $1/L3$), the signals on the short boom antenna are significantly larger in amplitude than that the long booms.
2. both signals show significant deviation from sinusoidal behavior (phase error) .



section4 Performance and Operation



Ambient ion density estimate (*top*) and axial E -field component (*bottom*) from particle and EFI. One can also see that the axial component of E is of similar, although lesser, magnitude to the spin plane components of E in this example (5 mV/m versus 10 to 20 mV/m, based on the peak-to-peak amplitudes of the spin plane E -field estimates in FIG).



section5 Summary



1. The THEMIS-EFI provides high-quality estimates of the DC electric field, allowing for accurate (better than 1 mV/m) estimation of the perpendicular E -field .
2. The DC measurement is susceptible to contamination by local electrostatic fields arising from cold plasma wakes, but the spin plane boom length differential allows for routine detection of this effect and monitoring of data quality.
3. The instrument supports 3D E -field measurements at frequencies up to 4 kHz, and provides significant supporting data for studies of large-scale electrodynamics as well as smaller-scale wave phenomena .